RESEARCH ARTICLE | SEPTEMBER 07 2022

Experimental investigation of combustion-induced starting hysteresis in the scramjet ⊘

Qifan Zhang (张启帆); Hao Chen (陈昊) ✉; Zhenjie Wu (吴振杰); ... et. al

⊙ Check for updates

CrossMark

🌐 View Online

⬇ Export Citation

Articles You May Be Interested In

Experimental investigation of unstart dynamics driven by subsonic spillage in a hypersonic scramjet intake at Mach 6
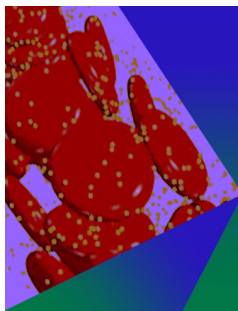
Physics of Fluids (February 2020)

Reciprocating and flapping motions of unstart shock in a scramjet isolator

Physics of Fluids (January 2022)

Hypersonic Inlet for a Laser Powered Propulsion System

AIP Conference Proceedings (November 2011)

Physics of Fluids

Special Topic: Flow and Forensics

Submit Today!

AIP Publishing

AIP Publishing

Experimental investigation of combustion-induced starting hysteresis in the scramjet

View Online   Export Citation   CrossMark

Qifan Zhang (张启帆),[1] Hao Chen (陈昊),[1,a] Zhenjie Wu (吴振杰),[2] Zhanbiao Gao (高占彪),[1] Weihang Luo (罗苇航),[1] Hongbin Gu (顾洪斌),[1] and Lianjie Yue (岳连捷)[1,a]

AFFILIATIONS

[1]State Key Laboratory of High Temperature Gas Dynamics, Institute of Mechanics, Chinese Academy of Sciences, Beijing 100190, China
[2]School of Engineering Science, University of Chinese Academy of Sciences, Beijing 100049, China

[a]Authors to whom correspondence should be addressed: chenhao@imech.ac.cn and yuelj@imech.ac.cn

ABSTRACT

Understanding the hypersonic inlet starting characteristics is the prerequisite for avoiding the abnormal unstart state. To make the work close to the actual situation, an experimental study was performed on a scramjet model at a simulated freestream Mach number of 6.0 with pressure and thrust measurements. The inlet working status is determined by the heat release of the injected ethylene with reciprocating variations. The results show that the critical equivalence ratio of the restart state is lower than that of the unstart state, which means that the combustion weakens the inlet restart capability and raises the unstart/restart hysteresis phenomena. Specifically, two novel unstart/restart hysteresis phenomena are found: one may come from the dual-solution characteristics of the shock–combustion interaction and the other may come from the historical effect of reverse flow. Compared to the former type, the latter type requires greater downstream heat release and generates a larger hysteresis loop. In addition, the engine thrust characteristics of the whole unstart and restart processes are analyzed. The thrust increment in the shock–combustion interaction type exhibits nearly linearly. However, the thrust increment meets abrupt changes and strong oscillations in the reverse flow type, accompanied by the reverse flow's formation and disappearance, making the engine more difficult to restart.

Published under an exclusive license by AIP Publishing. https://doi.org/10.1063/5.0103204

NOMENCLATURE

Ma	Mach number
p	Static pressure
t	Time
Φ	Equivalence ratio

Subscripts

t	Total
1	First cavity
2	Second cavity
0	Free stream

Superscripts

r	Restart state
s	Start state
u	Unstart state

I. INTRODUCTION

A hypersonic inlet, which is situated at the head of the flow path of the air-breathing propulsion system, connects the airframe and the propulsion system aerodynamically. Considering performance, combined with the starting problem, the mixed-compression inlet is the optimal option under hypersonic flow. The unstarted state is a typical abnormal mode of hypersonic inlets. Generally, when the internal flow does not alter the airflow capture characteristics of a hypersonic inlet, it is regarded as operating in a started mode; otherwise, in an unstarted mode.[1] The flight conditions, such as high back pressure of the combustor,[2] low flight Mach number,[3] large attack angle,[4] and sideslip angle, all might cause the hypersonic inlet to unstart. An unexpected unstart phenomenon may lead to violent shock system oscillation, prominent pressure fluctuation, and abrupt performance reductions that result in substantial engine thrust loss and even combustor flame-out.[5] Therefore, the unstart phenomenon should be avoided at any operation stage of hypersonic vehicles. Once the unstart phenomenon occurs, the interference factors should be eliminated to restart the inlet.

In general, the restart capability of the inlet is defined by whether the inlet can restart successfully after the unstart factors are eliminated. For this reason, the restart capability, as a key performance of the inlet, attracts a lot of research.

In recent years, many countries have put research into developing scramjets. However, the failure of the inlet restart after the unstart phenomenon occurred has been encountered in many famous scramjet flight tests, such as the joint test of the Central Institute of Aviation Motors and NASA in 1988[6] and the second flight test of X-51A performed by the U.S. Air Force in 2011,[7] leading to the unfulfillment of the task of these flight tests. Since Oswatitsch's first observation of the oscillatory aerodynamic phenomenon of supersonic inlets in 1944,[8] much work has been devoted to this particular subject for nearly 80 years. Tan et al.,[9,10] Wagner et al.,[11,12] Li et al.,[13] and Chang et al.[14] investigated the rectangular hypersonic inlet unstart process and periodic oscillation from downstream mass-flow choking. Similar work has been carried out on other types of inlets, such as axisymmetric inlets,[15] modular inlets,[16] and side compression inlets,[17] and some novel unstart phenomena[18–20] have been found and analyzed to enrich the understanding of hypersonic inlets. However, the starting problem of the inlet is still unpreventable in practice. This may result from the lack of a comprehensive understanding of the hypersonic unstart in the scramjet. Additionally, most current studies are based on aerodynamic research that deviates from the natural heat release of combustion in the scramjet.

The mass-flow choking induced by the plug is different from the thermal choking induced by combustion. The characteristic of downstream heat release will vary along with the upstream flow structure in real-time and give feedback to the upstream flow. In contrast, the effect produced by the downstream plug is mainly determined by local throttling conditions. Therefore, the combustion effect cannot be ignored in the unstart study and accurately represent the actual flight conditions. With the development of test facilities, researchers have tried to investigate the hypersonic unstart of the scramjet in high-enthalpy conditions.[21] Thermal choking behaviors and flow fluctuations during the unstart process were observed by O'Byrne.[22] Later, Laurence et al.[23,24] and Liu et al.[25] explained the transient and quasi-steady behaviors in fluid combustion phenomena using time-resolved imaging and pressure/temperature measurements. With the arc-heated hypersonic wind tunnel, Baccarella et al.[26] and Im et al.[27] investigated the unstart process triggered by mass loading and heat release. Severe

oscillatory flow motions of the unstart shockwave were observed in the combustion-driven unstart process. In contrast, the unstart shockwave under the cold free stream condition exhibited a relatively steady behavior. In addition, the mass spills in the unstart state will affect the pressure by changing the jet flow structure and the heat release simultaneously. Unfortunately, due to the limited usable runtime, these studies are only focused on flame-flow dynamics in the unstart process. In the study on the starting problem driven by combustion, the equally important restart process has not received the attention it deserves.

The restart process will present different characteristics corresponding to the different kinds of unstart trigger factors.[28,29] Specifically, due to the mass-flow choking in the throat brought by the total pressure loss of the restart cowl shock, a hysteresis phenomenon of inlet start/unstart can be found in the restart process corresponding to the flight Mach number and attack angle.[30] It must be noted that the hysteresis will disappear while the inlet has the restart capability examined by the traditional aerodynamic method.[31] However, Chang[32,33] conducted research on the hysteresis characteristics in the changing of the equivalence ratio (ER), which indicated an obvious hysteresis effect in the inlet mode transition. To restart the inlet, the fuel supply should be decreased too far less than that of the critical state in the start-to-unstart transition due to the hysteresis effect. Thus, it can be seen that combustion may change the inlet start capability. However, such an experiment is carried out with the direct-connect scramjet experiment system. The converging duct acting as a simplified inlet cannot simulate the mass spillage of the unstart state in the real scramjet.

In summary, there is a lack of understanding of the unstart and restart processes driven by combustion in the scramjet and the comparison of the two corresponding processes. Furthermore, the research should be more representative of the actual scramjet working conditions to support the engineering application. Therefore, the current paper experimentally investigates the start-to-unstart and the unstart-to-restart processes with a scramjet model through fuel supply variation.

II. EXPERIMENTAL APPROACH

A. Variable Mach number hypersonic propulsion test facility

The experiments were performed at the variable Mach number hypersonic propulsion test facility of the Institute of Mechanics, Chinese Academy of Sciences. This facility, shown in Fig. 1, can

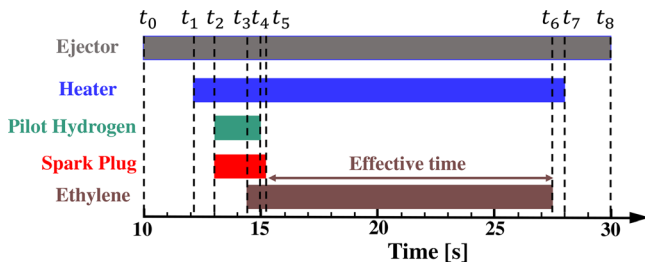**FIG. 1.** The variable Mach hypersonic propulsion test facility.

FIG. 2. Brief description of the experimental steps and the time sequence.

FIG. 4. Schematic of the cavity.

simulate the inflow conditions of a maximum total temperature of 1950 K and a total pressure of 6 MPa within an effective operating time of 100 s. The outlet size of the wind tunnel nozzle is $330 \times 330 \, mm^2$, providing nominal freestream Mach numbers from 4.5 to 6.5, while the actual range can be larger. To obtain high total temperature and total pressure, hydrogen is burned with air in the heater while oxygen is supplied to maintain a 21% mole fraction of oxygen. The stagnation parameters of the incoming flow can be varied by adjusting the mass flow rates of hydrogen, oxygen, and air. Specific test conditions will be given in the test condition section.

The following is a brief description of the experimental procedures and the time sequence in this paper in conjunction with Fig. 2. At the start of the test, the ejector will be the first to turn on to establish the vacuum condition required for the nozzle to start. Once the vacuum is stabilized, the heater will operate to create a steady high enthalpy incoming flow and establish the initial wind tunnel flow field from time t_1. Subsequently, pilot hydrogen is injected into the combustor and ignited by spark plugs. The easy ignition and high calorific value of hydrogen are used as a high-energy ignition source to ignite the subsequent injection of ethylene fuel. When stable combustion of ethylene is obtained, the pilot hydrogen injection will be turned off to ensure that the subsequent period is a pure ethylene burning phase for the effective test time. During this period, the ethylene fuel injection will also be adjusted according to the preset adjustment strategy. To simulate the unstart and restart processes of the scramjet in the same test, the effective test time needs to be set long enough. The entire pure ethylene test time is approximately 13.0 s, starting from $t_5 = 15.0 \, s$ and ending at $t_6 = 28.0 \, s$.

B. Scramjet model and test conditions

The scramjet model studied in this paper has a total length of approximately 2.0 m, including the inlet, isolator, combustor, and nozzle. The structure and dimensions are shown in Fig. 3. The inlet adopts a two-stage compression design of a 6° oblique shock wave and a 4.5° isentropic wave, with a capture area of $150 \times 80 \, mm^2$. The inlet throat

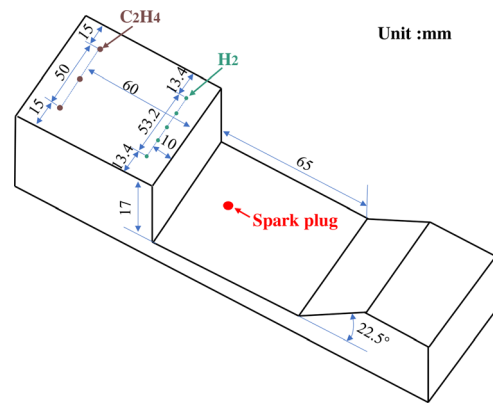is 40 mm high, and an isolator 240 mm long directly follows the throat. The combustor behind the isolator has a constant-width expansion structure with an expansion angle of 2.8°. Behind the combustor is the nozzle, with a length of 396 mm. The nozzle expands to 150 mm in exit height, which is the same as the capture height of the inlet. The flow channel in the combustor is a constant 80 mm wide. The combustor adopts a double-row four-cavity structure, and the cavities on the upper and lower walls are designed symmetrically in the flow direction. The specific structure of a single cavity and the size of the injection holes are shown in Fig. 4. The depth, length, and angle of the trailing edge of the cavities are 17 mm, 65 mm, and 22.5°, respectively. The ethylene and hydrogen injection holes are located 60 and 10 mm upstream of the cavity. The igniters are located at the bottom of the cavities. Each ethylene injector has circular cross sections with the same diameter of 2.0 mm. In addition, water-cooling channels are set in the isolate, combustor, and nozzle sections with a high heat load to match the long test time.

To improve the starting ability of the wind tunnel and maintain the uniformity of the engine inlet flow field, the inlet of the scramjet model was designed as a truncated inlet. Specifically, this paper removes the first-stage 6° compression from the previously designed three-stage compression inlet and retains only the subsequent two-stage compression. Then, the internal flow path is turned to the level of the first-stage compression surface to obtain the above two-stage compression truncated inlet. Corresponding to the truncated inlet, the incoming flow parameters of the wind tunnel will also be adjusted to the flight incoming flow conditions compressed by 6.4°, considering the additional effect of the boundary layer. Therefore, the test Mach number was set as 5.1 to simulate a flight Mach number of 6.0, and the specific parameters are shown in Table I. In the following
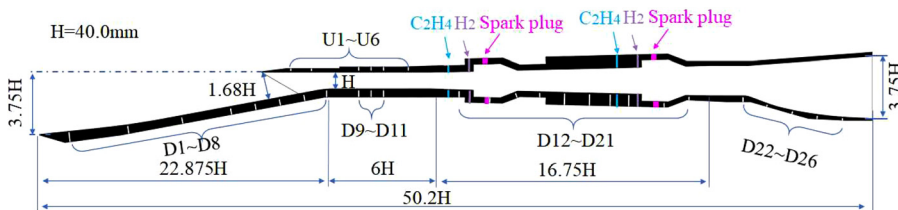

FIG. 3. Geometric parameters of the scramjet model.

TABLE I. Correspondence between flight condition and test facility flow condition.

Flight condition				Test condition			
Mach number	Statice pressure (kPa)	Total temperature (K)	Total pressure (MPa)	Mach number	Statice pressure (kPa)	Total temperature (K)	Total pressure (MPa)
6.0	2.11	1513	3.88	5.1	5.06	1513	3.63

description and analysis, the flight Mach number will be used to characterize the test condition to avoid confusion between the simulated flight Mach number and the actual test Mach number. In addition, a rectangular nozzle extension cover with a half-open structure is installed at the nozzle outlet in Fig. 5 to extend the nozzle uniform area to cover the engine inlet. Furthermore, two oblique baffles are added on both sides of the inlet front body to avoid the impact of the three-dimensional flow and obtain the two-dimensional flow field for the inlet. It must be noted that the inlet part has the capability to restart under the test condition by the aerodynamic assessment means.

C. Measurement facilities

Since the test in this article involves multiple systems, both the test facility and the scramjet model are equipped with multiple test systems. The following will be introduced one by one. The first is the system of the facility. To monitor the incoming flow, the pressure sensor of "UNIK 5000" General Electric with a pressure measurement accuracy of 0.1% Full Scale (herein abbreviated as "FS") was installed upstream of the nozzle. Ethylene fuel undergoes dynamic adjustment of the equivalent ratio through an electric pressure reducing valve, and its flow rate is obtained with a differential pressure orifice flowmeter. The differential pressure transmitter has a range of 0.4–40 kPa and an accuracy of 0.1% FS, which can ensure high-precision flow measurement.

For the scramjet model, the wall pressure and the direct thrust measurements are used mainly to obtain the internal flow field and performance of the engine. Specifically, as shown in Fig. 3, six pressure measuring points labeled U1–U6 are set on the cowl side, and twenty-six measuring points marked D1–D26 are set on the ramp side. Wall pressure is measured with the DTC Initium ESP-32HD electronic pressure scanning module with 0.25% accuracy and a sampling frequency of 652 Hz. Because of the lower pressure of the inlet and nozzle than the combustor, a range of 45 PSI electronic pressure scanning

modules is used in the inlet and nozzle section. In comparison, a range of 100 PSI electronic pressure scanning modules is used in the combustor section. The "13-CYZH-02A" cassette strain gauge balance of the AVIC Aerodynamics Research Institute is placed under the scramjet model to obtain the dynamic variation process of the engine thrust. The specific axial force range of the balance is ±4000 N with a standard measurement uncertainty of 0.30% FS. The balance signal is acquired by the DH5939E high-frequency signal acquisition system of Donghua Testing Technology Co., Ltd., with a sampling frequency of 5 kHz. In addition to the above-measuring methods, two pressure sensors are installed on hydrogen and ethylene fuel supply pipes to monitor fuel injection pressures and timing. The two sensors are recorded at 1000 Hz by the "Pacific Instruments series 6000" data acquisition system. Moreover, all experimental data acquisitions are triggered by the same TTL (transistor–transistor logic) signal source to ensure the recording time consistency of these data. More details of the facility, test-section model, and measuring methods can be found in a prior study.[34]

III. RESULTS AND DISCUSSION

Considering the shorter distance between the inlet and the first row of cavities, the working status of the inlet is more susceptible to the combustion of the first row of cavities than the second. Therefore, a reciprocating variation is set to the ER of the first row of cavities. Meanwhile, the ER of the second row of cavities remains a constant value to reduce variables. Specifically, the ER adjustment parameters of the test conditions are summarized in Table II, in which Φ_1, Φ_2, and Φ_t denote the ethylene ER injected upstream of the first cavities, ethylene ER injected upstream of the second cavities, and the total ER, respectively. To simulate the unstart and restart process, the reciprocating variation of ER can be divided into three typical stages: the early ER increase stage, the middle ER steady stage, and the later ER decrease stage. In addition, the operation condition of the inlet should be the start state with the initial ER and the unstart state with the maximum ER, resulting in a relatively wide range of ER variations. Different ER adjustment strategies are designed to investigate the influence of the combustion intensity on the characteristics of the unstart and restart phenomena and the coupling effect of the multi-cavities structure. Due to the limitation of the test facility and the
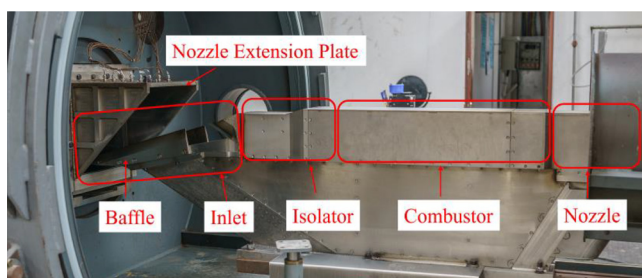

FIG. 5. Scramjet model mounted on the test section of the variable Mach hypersonic propulsion test facility.

TABLE II. Experimental parameters for all test cases.

Test case	Flight condition	Φ_1	Φ_2	Φ_t
A1	Ma6.0	0.12–0.42–0.12	0.21	0.33–0.63–0.33
A2	Ma6.0	0.10–0.55–0.10	0.46	0.56–1.01–0.56

water-cooling test model, the optical path cannot be established to observe the entrance of the inlet. Therefore, the commonly used Schlieren method for judging the operation condition of the inlet is not available in this experiment. Thus, in this paper, the pressure of point D7, located immediately downstream of the backward sidewalls of the inlet, is used to judge the inlet operation condition. While the inlet transitions from the start state to the unstart state, the pressure of point D7 will start increasing due to the mass spillage through the sidewalls at the inlet entrance. Conversely, the pressure of point D7 will decrease to the initial value once the mass spillage disappears, which means the inlet transitions from the unstart state to the start state.

A. Unstart and restart processes of the scramjet

To have an overview of the unstart and restart processes of the inlet, Fig. 6 presents the static pressure histories of survey points D4–D7, located near the inlet entrance, during the three stages of ER. The top half of Fig. 6 shows the histories of Φ_1, Φ_2, and Φ_t. The fuel dynamic supply system has satisfactory linearity and repeatability in the early increase stage and the later decrease stage. In contrast, the pressure data do not exhibit relative linearity and repeatability corresponding to ER. To make the comparative analysis, the critical times, defined by the pressure of survey point D7, of the start-to-unstart transition and the unstart-to-restart transition are labeled with purple lines in Fig. 6. A significant difference can be found in the ERs corresponding to the critical times in the two tests. This means that an apparent hysteresis phenomenon exists in the inlet mode transition process. In other words, the combustion effect changes the inlet start capability.

Specifically, at the initial stage with $\Phi_1 = 0.12$, the inlet is working at the start state from 15.0 to 16.65 s in test A1 [Fig. 6(a)]. During the ER increase stage, from 16.65 to 20.2 s, the pressure at point D7 increases rapidly at 18.73 s with $\Phi_1 = 0.30$, indicating that the inlet transitions from the start state to the unstart state driven by the downstream back pressure. Subsequently, the combustion pressure increases and propagates upstream to survey points D6 and D5 in turn. The pressure of survey points D5–D7 increases rapidly at first, and then the pressure increase slows down significantly after 19.35 s with $\Phi_1 = 0.35$. At the ER steady stage, from 20.20 to 22.05 s, an interference

fluctuation can be found in survey point D5 compared to the stability of survey points D6 and D7. This shows that there is still a relatively long flow equilibrium process at the inlet of the engine even when the downstream combustion is stabilized. During the ER decrease stage, from 22.05 to 25.6 s, the D7 pressure stops falling at 24.23 s with $\Phi_1 = 0.23$, indicating that the inlet transitions from the unstart state to the restart state.

In test A2 [Fig. 6(b)], with a larger variation amplitude of ER, deviation also exists between the critical values of the different inlet mode transition processes. Furthermore, the degree of deviation increases in test A2 compared to test A1. Meanwhile, significant changes can be found in the characteristics of the pressure near the inlet entrance. Driven by the higher combustion pressure, the downstream disturbance propagates upstream of survey point D4 at the early ER increase stage. At the ER steady stage, an abrupt increase occurs at survey point D7, and the pressure ratio increases rapidly from 20 to 60, accompanied by a significant increase in pressure fluctuation. In contrast, the pressure of the upstream survey points D5 and D6 does not exhibit similar abrupt changes or significant oscillations. This novel phenomenon again proves a relatively long flow equilibrium process at the inlet after the engine transitions to the unstart state. On the other hand, the inlet flow field may meet sudden changes under different unstart degrees. Such characteristics are quite different from the previous understanding of the inlet unstart state based on aerodynamic research. Subsequently, detailed comparison and analysis will be conducted based on the specific pressure distribution along the flow path.

Since there is an obvious unstart/restart hysteresis in the upstream inlet, how will the pressure in the downstream combustor change? How will the variation in combustor pressure react to the inlet flow field? To answer these questions, Fig. 7 presents the static pressure histories of specific survey points in the combustor, accompanied by survey point D7 for comparison. In this figure, the survey points D11, D13, D17, and D20 are located in the isolator, inside the first cavity, between the two cavities, and inside the second cavity, respectively. In test A1, after the inlet transitions to the unstart state, a low-frequency and significant amplitude fluctuation can be found in survey point D11, which may be caused by the unsteady sweep of the shock train in the isolator. The amplitude of the disturbance increases with
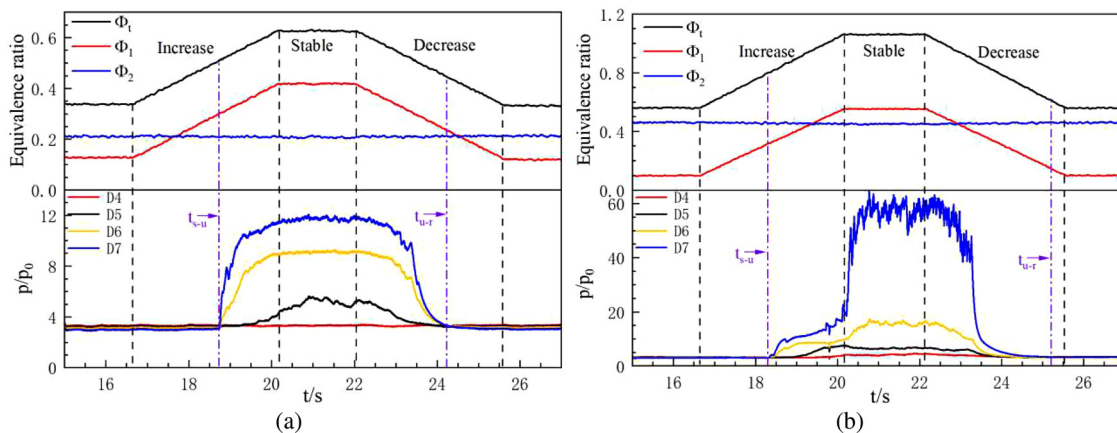

FIG. 6. Pressure of the survey points near the entrance and ER vs time. (a) Results of test A1. (b) Results of test A2.
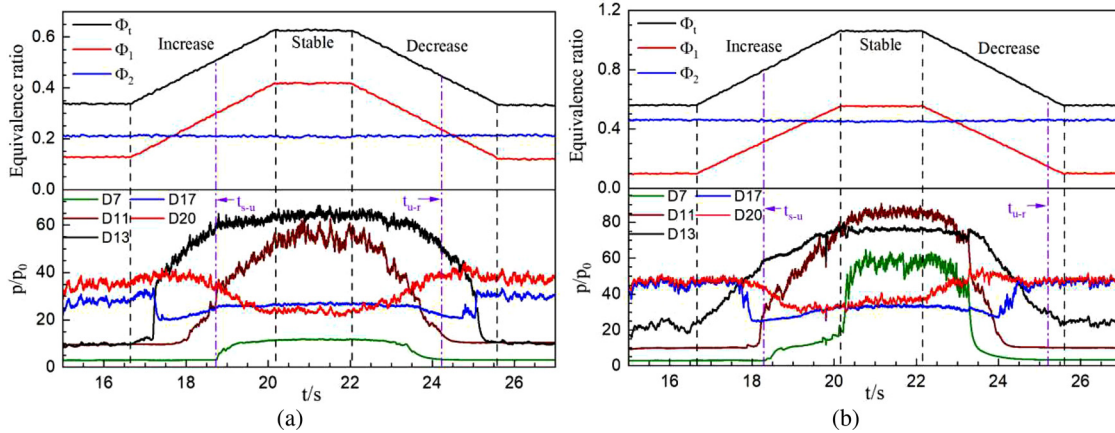
FIG. 7. Pressure of the survey points in the combustor and ER vs time. (a) Results of test A1. (b) Results of test A2.

the deepening of the unstart degree. However, the disturbance will not be amplified through the combustion region of the first cavities. It is speculated that the thermal throat formed by intense combustion in the first cavities has a specific filtering effect on the upstream disturbance. Therefore, the high amplitude of the disturbance only exists in the isolator between the inlet and the first cavities. Then, in test A2, Φ_t increases from 0.56 to 1.01, which is larger than the variation range of 0.33–0.63 in test A1. As a result, the low frequency and significant amplitude fluctuation found in the isolator of test A1 is inexistent in test A2 at the steady stage. In addition, the measuring point with the most significant pressure amplitude in the engine flow path is changed from point D11, located in the isolator of test A1, to point D7, located at the entrance of the inlet in test A2. From this, it can be speculated that the disturbance characteristics of the flow field are different in the two tests. In other words, a new source of the disturbance has been established in test A2. As in test A1, the disturbance will not be amplified through the combustion of the first cavities and filtered by the thermal throat. Therefore, the abrupt change formed upstream at 23.25 s cannot propagate downstream through the first cavities. In other words, the start characteristics of the inlet are mainly affected by the combustion effect of the first cavities. In contrast, the combustion effect of the second cavities is isolated by the intense combustion effect of the first cavities.

To quantify the starting hysteresis of the inlet, the critical ERs corresponding to the start-to-unstart process and the unstart-to-restart process are presented in Table III. The deviation between the critical ERs of the unstart state (Φ_t^u) and the restart state (Φ_t^r) is defined as $\Delta\Phi_h$, representing the size of the start/restart hysteresis loop of the engine. As mentioned before, the combustion of the first cavities has a

decisive influence on the start characteristics of the inlet, so the critical ERs of the first cavities are the more typical parameter than the others, which will be mainly discussed below. Specifically, Φ_1^u in the two tests are 0.30 and 0.31, respectively, and are almost the same. On the other hand, Φ_1^r in the two tests are 0.23 and 0.15, respectively, showing an obvious difference. As a result, $\Delta\Phi_h$ of test A2 reaches 0.16, which is much higher than 0.07 in test A1.

For further analysis, Fig. 8 exhibits the distributions of the time-averaged surface pressures at the critical moments of the unstart and restart states. The pressure average of seven representative pressure values near the selected time is used to eliminate the influence of pressure fluctuation. In addition, the pressures are normalized by the free-stream static pressure of the corresponding moment. First, two peak pressures can be found around the two-row cavities along the flow path at the critical moments of the unstart state in the two tests. The first peak pressure around the first cavities is almost the same in the two tests for the approximate Φ_1^u, while the second peak pressure is different for the deviation of Φ_2. In addition, the rapid decrease in the pressure distribution downstream of the first cavities indicates supersonic flow formation for the strong combustion effect in the first cavities. The supersonic flow will isolate the disturbance of the second cavities. That is why the Φ_1^u values in the two tests are almost the same, while the corresponding Φ_2 values are different. Two peak pressures can be found at the critical time of the restart state in test A1 in Fig. 8(b), similar to the critical time of the unstart state in test A1 in Fig. 8(a). However, the overall value of the restart state is lower than that at the critical time of the unstart state, and the high pressure in the combustor is reduced simultaneously. On the other hand, in test A2, there is only one peak around the second cavities in the pressure distribution along the path for the relatively low Φ_1^r. Because of the significant difference in the pressure distribution characteristics at the critical time of the restart state in the two tests, the restart processes are quite different in the two tests, which is the focus of the analysis in Sec. III B of this paper.

B. Mechanism of the hysteresis

As mentioned before, the inlet has the capability to restart under the condition of Ma 6.0 by the aerodynamic assessment means.

TABLE III. ERs at the critical time in the transition process.

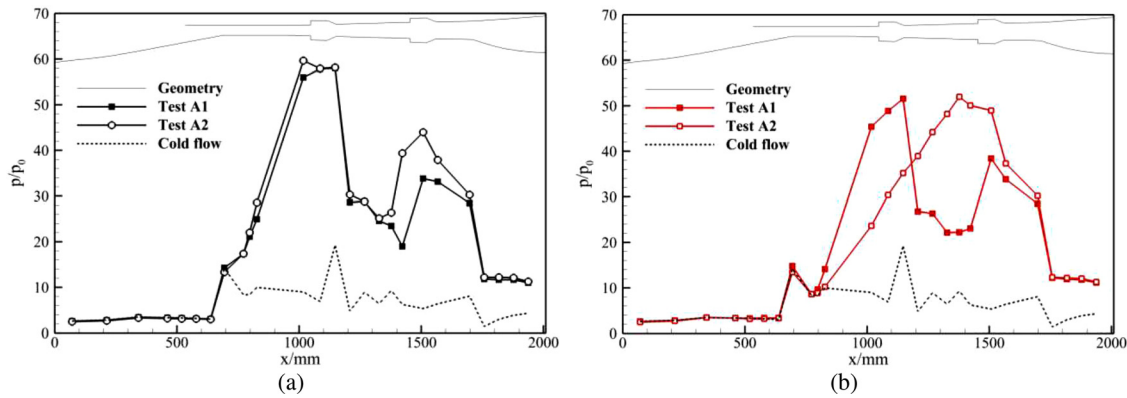| Test	Start-to-unstart			Unstart-to-restart			$\Delta\Phi_h = \Phi_t^u - \Phi_t^r$
	Φ_1^u	Φ_2	Φ_t^u	Φ_1^r	Φ_2	Φ_t^r	
A1	0.30	0.21	0.51	0.23	0.21	0.44	0.07
A2	0.31	0.46	0.77	0.15	0.46	0.61	0.16

FIG. 8. Pressure distribution at the critical time in the transition process. (a) Critical time in the start-to-unstart process. (b) Critical time in the unstart-to-restart process.

However, a novel unstart/restart hysteresis phenomenon is found in our tests, which means that the combustion effect of the scramjet will weaken the inlet restart capability. To explore the mechanism of the new hysteresis phenomenon, the flow field evolution in the transient of the unstart and restart processes will be analyzed and discussed in the comparison below.

To enhance comparability, Fig. 9 exhibits the distributions of the transient surface pressures corresponding to typical ERs in the increase and decrease stages of test A1. Due to the decisive influence of the combustion in the first cavities, Φ_1 is selected as the variable in Fig. 9. The solid lines represent the ER increase stage, and the dotted lines represent the ER decrease stage. First, in the increase stage, there are two peaks along the pressure distribution at $\Phi_1 = 0.20$; the first is located at the back edge of the first cavities, and the second is located at the injection region of the second cavities. As Φ_1 increases to 0.32, the inlet transitions into the unstart state. There are still two peaks along the pressure distribution. During the ER increase process, the pressure in the first cavities continuously increases, while the pressure at the second cavities decreases instead. Based on the previous analysis, the pressure increase in the first cavities indicates that the thermal throat generated by the combustion is strengthened, and downstream

supersonic flow is accelerated continuously. Under the double effect of the oxygen consumption increase and the local supersonic flow acceleration, the combustion of the second cavities is weakened, accompanied by a pressure decrease. As Φ_1 increases to 0.42, the pressure in the first cavities reaches the maximum level, and the value in the second cavities reaches the minimum level. After the steady stage of $\Phi_1 = 0.42$, the ER decrease stage occurs. At the unstart state of the inlet in the ER decrease stage, the pressure distributions along the inlet and the isolator at ERs of 0.27, 0.32, and 0.37 are slightly higher than in the ER increase stage. In addition, the pressure rise point is located more upstream in the flow path. Such pressure deviation does not vanish until the inlet transitions from unstart to restart at $\Phi_1 = 0.20$. Hence, the cause of the deviation is the key to the unstart/restart hysteresis phenomenon in test A1.

From the above, there are two slightly different pressure distributions at the same ER at different ER variation stages, which is similar to the phenomenon in the scramjet combustor found by our group with the numerical simulation[35] and direct-connect experiment.[36] Two different pressures in the cavity come out at the same equivalent ratio, which means the flow field appears dual-solution characteristic. Specifically, a kind of hysteresis is located in the jet-wake stabilized mode, which can be attributed to the flame/shock interaction mode transitions between the flame/shock weak interaction mode and the flame/shock intensive interaction mode. Different modes result in a slightly stronger/weaker flame along with larger/smaller flow separation and show slightly higher/lower pressure rises near the cavities and upstream/downstream movement of the pressure-rise origin. And that is the result of the difference in the combustion efficiency for the difference in the fuel mixing and reaction velocity under the different flow fields. In the historical ER increase path, the initial flame/shock weak interaction mode had a smaller flow separation, indicating a slightly lower combustion efficiency. The ER should exceed a slightly higher critical value to generate enough heat release for higher combustion zone pressure increases to induce a change in the shock/flow separation structure. Then, it transitioned to the flame/shock intensive interaction mode. However, in the historical ER decrease path, the initial intensive interaction mode had a larger flow separation, indicating a slightly higher combustion efficiency. The ER should decrease below a slightly lower critical value to generate heat release, which is not enough to maintain the current shock/flow separation structure, and
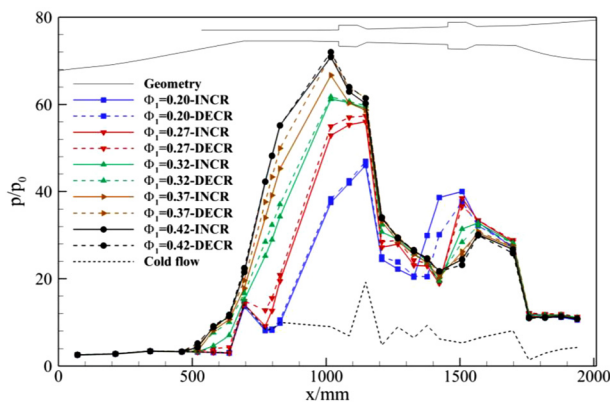

FIG. 9. Pressure distribution along the ramp side at typical ERs at different stages in test A1.

then the inverse transition occurs. The difference between the two critical transition ERs resulted in the hysteresis loop. Therefore, the combustion field will show a significant hysteresis phenomenon due to the historical effect, which is a novel characteristic of the combustion field compared to the aerodynamic field. The dual-solution characteristics caused by the combustion efficiency are consistent with the results in test A1 in this paper, which is quite different from the hysteresis phenomenon found by the traditional aerodynamic method. Therefore, we speculate that the starting hysteresis of the engine in test A1 is caused by the dual-solution characteristics of the shock–combustion interaction. Based on the currently limited data, the understanding is still relatively superficial, and this part of the research needs to be followed up with more systematic and detailed work.

Figure 10 exhibits the distributions of the transient surface pressures corresponding to typical ERs in the increase and decrease stages of test A2. As Φ_1 increases from 0.10 to 0.55, the pressure distribution evolves from a single pressure peak at the second cavities to double pressure peaks at the first and second cavities. The pressure of the first cavities is higher than that of the second cavities. Subsequently, the maximum pressure area in the flow path is gradually transferred from the second cavities to the isolator. The pressure near the second cavities stops decreasing once ER increases to a specific value. The characteristics of the pressure variation of test A2 and test A1 are similar in the early increase stage, but there is a significant difference in the later stages. In the maximum ER steady stage from 20.2 to 22.0 s, an abrupt rise occurs at survey point D7. As a result, the pressure distribution at $\Phi_1 = 0.55$ in the decrease stage shown as the dashed line is much higher than the corresponding value in the increase stage, shown as the solid line. The third peak of pressure appears in the contraction section of the inlet, which means the flow field of the unstart state has met significant change. Such flow field is maintained until Φ_1 decreases to 0.35 with the abrupt decrease in pressure of survey point D7. Under the influence of the flow field, the corresponding pressure distribution along the flow path in the ER decrease stage is higher than that in the ER increase stage. In other words, the flowfield strengthens the combustion at the first cavities to a certain extent, and the high back pressure generated by the enhanced combustion is also the key to maintaining the flowfield.
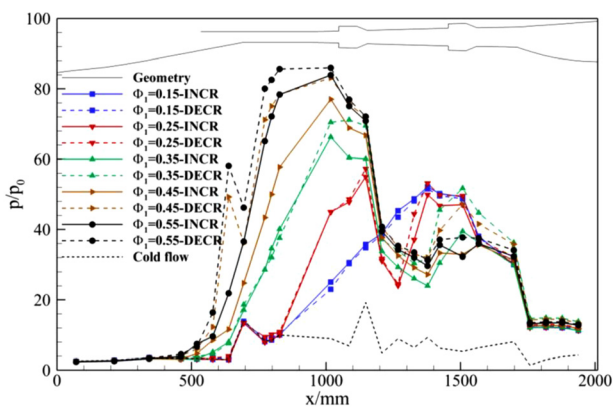
To analyze the two abrupt changes of survey point D7 in test A2, Fig. 11 presents the pressure distributions along the flow path before and after the two abrupt changes. The solid lines represent the abrupt increase moment, and the dotted lines represent the abrupt decrease moment. The red lines correspond to the relatively high level of D7 pressure, and the black lines correspond to the relatively low level of D7 pressure. At the abrupt increase phase at 20.2 s, there is no similar abrupt change in the pressure at the upstream and downstream survey points. That is to say, the abrupt increase in survey point D7 is affected by the propagation of high pressure in the combustor. The abrupt change in the flow field is limited to the inlet section. At this moment, the "V" shape pressure distribution formed by survey points D7, D8, and D9 is speculated to indicate that the reverse flow appears at the throat. Considering inlet working status is decided by the pressure propagation, the inlet unstart flow fields induced by the thermal choking and mass-flow choking are similar in qualitative. In our previous research,[37] we found a reverse flow with detached normal shock, resulting in a local high pressure upstream of the inlet, which is quite similar to the results in our current paper. Driven by downstream high backpressure, the reverse flow that existed at the entrance is accelerated to supersonic by the expansion fan around the shoulder of the inlet. The reverse and incoming flow meet near survey point D7, inducing a positive shock wave. According to the inference, the pressure ratio after the positive shock wave can be estimated at 69 times the static flow pressure, which is close to the pressure ratio of approximately 60 after the abrupt rise of survey point D7. This further supports the speculation about the existence of reverse flow. On the other hand, the reverse flow should be instantaneous, or the flame in the combustor will go out. Therefore, the reverse flow may accompany strong oscillations in accord with the pressure fluctuation in Fig. 6(b). At the abrupt decrease phase of D7 at 23.25 s, the pressure in the inlet and isolator section meets a significant drop simultaneously. The influence range of the abrupt change in the decrease phase is much larger than that in the increase phase. Thus, the abrupt change in the pressure will greatly impact the thrust and torque of the engine, which will greatly increase the difficulty of controlling the restart of the engine.

Based on the above analysis, the reverse flow in test A2 vanishes as Φ_1 decreases to 0.4, and the value of 0.4 is higher than $\Phi_1^r = 0.23$ in test A1. In other words, if the historical effect of the reverse flow
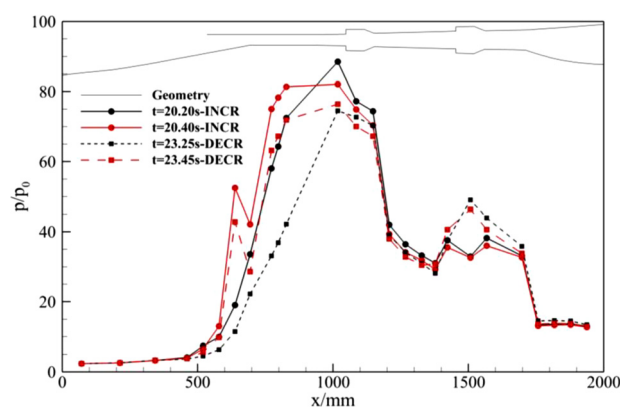

FIG. 10. Pressure distribution along the ramp side at typical ERs at different stages in test A2.

FIG. 11. Pressure distribution before and after the two abrupt changes of survey point D7 in test A2.
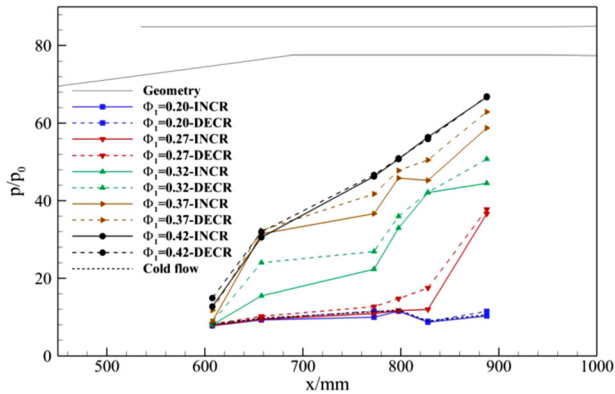
FIG. 12. Pressure distribution along the cowl side at typical ERs at different stages in test A1.

pattern ends at $\Phi_1 = 0.40$, Φ_1^r of test A2 should be the same as test A1. However, according to Table III, Φ_1^r of test A2 is 0.15, which is significantly lower than $\Phi_1^r = 0.23$. Therefore, the historical effect of reverse flow does not disappear with the disappearance of reverse flow and will continue to affect the subsequent restart process. Let us turn back to Fig. 10. The pressure distributions of $\Phi_1 = 0.25$ and $\Phi_1 = 0.35$ in the ER increase and decrease processes are relatively close in the combustor, which means that the difference may occur in the inlet section. For this reason, the pressure distributions along the cowl side at typical ERs in the increase and decrease stages of the tests are presented in Figs. 12 and 13. As shown in Fig. 12, the high-pressure ratio will decrease as ER decreases, and the high-pressure region will recede downstream. Similar to Fig. 9, the pressure distributions along the cowl at the ER decrease stage are slightly higher than those at the increase stage. The deviation does not vanish until the ER decreases to 0.20, corresponding to the start state. In addition, the distribution laws of the pressure along the cowl side are similar at the same ERs in the different processes, which means that the flow structure is similar. This is consistent with the previous analysis of test A1. Compared with the result of test A2 in Fig. 13, significant differences still exist in the pressure at the same ER in the region between the reverse flow
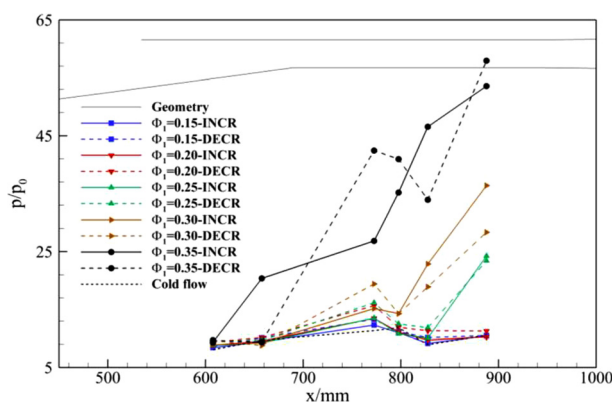

FIG. 13. Pressure distribution along the cowl side at typical ERs at different stages in test A2.

vanishing and inlet restart, while Φ_1 varies from 0.40 to 0.15. The pressure of survey point U3 located in the throat is kept at a high value, while the other points have decreased to a relatively low value, which means there may be a separation at the throat of the inlet. The formation of the separation is suspected to be induced by the preceding reverse flow with oscillation, and the separation does not vanish until the ER drops to a relative low value.

In summary, there are two kinds of unstart/restart hysteresis phenomena driven by the combustion of the scramjet. One may come from the dual-solution characteristics of the shock–combustion interaction, and the other may come from the historical effect of reverse flow. The occurrence of the two hysteresis phenomena is strongly determined by the ER variation range. Compared to the shock–combustion interaction type, the occurrence of the reverse flow type requires greater downstream heat release and generates a larger hysteresis loop. Therefore, much attention should be given to the flow mechanism and engineering adjustment for the reverse flow type.

C. Characteristics of the thrust variation

As the parameter of the scramjet engine, how thrust varies during the unstart and restart process is quite important and has not been considered in previous studies. Moreover, the pressure distribution characteristics described and discussed above will directly affect the engine thrust. With the help of the cassette strain gauge balance, the joint forces of the scramjet model can be measured. However, the joint forces include the external resistance and internal resistance in addition to the thrust. To obtain the evolution characteristics of the engine thrust, we need to remove such interference factors by carrying out the no-fuel test. By reducing the reference value of the no-fuel test, the thrust increment time histories of the tests are presented in Fig. 14. To better obtain the nonlinear characteristic of the thrust, the thrust data are subjected to 6 Hz low-pass filter processing to remove the fluctuation disturbance. In addition, the histories of Φ_1, Φ_2, and Φ_t have been added to the figures. The critical times of the start-to-unstart transition and the unstart-to-restart transition are labeled with purple lines.

Overall, the change characteristics of the thrust increment in tests A1 and A2 are different. The thrust increment in test A1 [Fig. 14(a)] exhibits a nearly linear change with the ER variation. No abrupt change occurs at the critical state in the start-to-unstart transition or unstart-to-restart transition. Furthermore, the thrust increment of the engine will continually increase with increasing ER and vice versa. Therefore, it can be concluded that the unstart state of the inlet, which is defined by the airflow capture characteristics, cannot determine the change characteristics of the engine thrust. In addition, due to the high-pressure sustentation of the combustor, the engine thrust increases continually rather than decreases at the relatively low degree of unstart state. As discussed in Fig. 9, during the unstart stage, the pressure distributions along the inlet and the isolator at the ER decrease stage are higher than those in the ER increase stage. Considering the compression surface of the inlet is the resistance surface, the higher pressure along the compression surface indicates a higher drug produced. As a result, the value of the thrust increment at the decrease stage is slightly lower than that in the increase stage.

Compared to test A1, the change characteristics of the thrust increment in test A2 [Fig. 14(b)] are more complicated and accompanied by fluctuations. According to the above analysis, the pressure
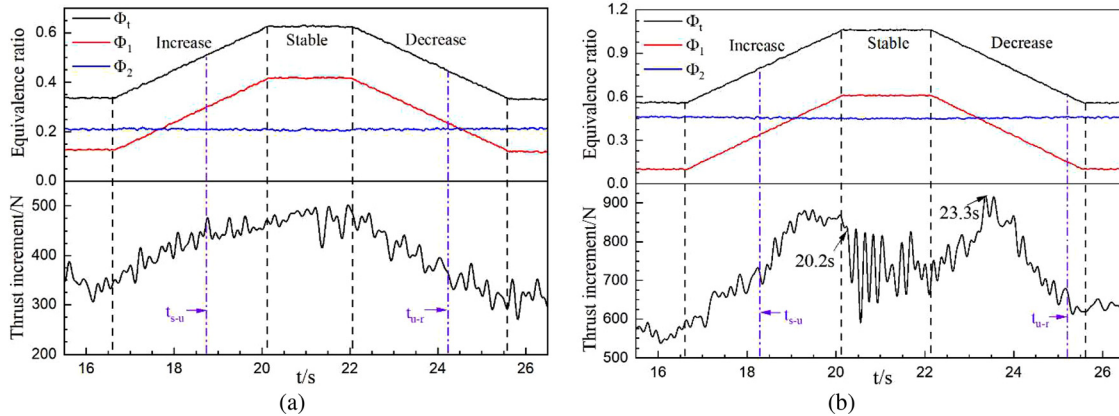
FIG. 14. Thrust increment and ER vs time. (a) Results of test A1. (b) Results of test A2.

along the inlet and combustor increases continually in the ER increase stage. With the deepening of the unstart degree, the negative effect of the compression surface increases, eliminating the active effect of the combustor on the engine thrust. Therefore, in the ER increase stage, the thrust increment increases overall, and the rate of the increase reduces significantly near the end. Subsequently, an abrupt drop and large oscillation occur at the beginning of the steady stage, consistent with the abrupt change in survey point D7 in Fig. 6. The high-pressure zone formed at the compression side of the inlet in Fig. 11 has a significantly negative effect on the engine thrust. Such abrupt change and oscillation of the engine thrust are catastrophic to the vehicle. In the subsequent ER decrease stage, the thrust increment starts to increase due to the shrinking amplitude and range of the high-pressure zone in the inlet. At $t = 23.25$ s, the thrust increment reaches the maximum value of the decrease process at the critical moment when the reverse flow disappears. After that, the thrust decreases linearly as ER decreases.

In summary, the occurrence of reverse flow will significantly affect the thrust increment variation. The change characteristics of the thrust increment in test A2 are irregularly and accompanied by abrupt changes and oscillations. Once the unstart/restart hysteresis phenomenon accompanied by the reverse flow occurs in actual flight, the thrust variation coupling with the flight speed, height, and attitude of the vehicle, will make the engine more difficult to restart.

IV. CONCLUSION

To enrich the understanding of the starting characteristics in the scramjet, we performed an experimental study on a scramjet model with two rows of cavities at the simulated freestream Mach number of 6.0. The working status of the inlet is generated by the heat release of the injected ethylene. The unstart and restart processes of the scramjet are performed in the same test to enhance comparability. Accordingly, reciprocating variations are set to the ER of the first row of cavities, namely, Φ_1. Meanwhile, the ER of the second row of cavities remains a constant value to reduce variables. With the aid of pressure and thrust measurements, the transient flow pattern and characteristics of the engine were recorded.

The variation of Φ_1 can be divided into three typical stages: the early increase stage, the middle steady stage, and the later decrease stage. The fuel dynamic supply system has satisfactory linearity and repeatability in the increase and decrease stages. In contrast, the pressure data do not exhibit relative linearity and repeatability similar to ER. The critical ER of the restart state is lower than that of the unstart state, which means that a novel unstart/restart hysteresis phenomenon is found in the tests. It should be noted that the inlet has the capability to restart under the condition of Ma 6.0 by the aerodynamic means of assessment. In other words, the combustion effect of the scramjet will weaken the inlet restart capability. Therefore, the fuel supply should decrease to a lower level than that in the unstart critical state.

According to the experimental results, the inlet working status is strongly determined by the combustion in the first row of cavities. With the adjustment of the ER, two different unstart/restart hysteresis loops are found with the same unstart critical ERs and different restart critical ERs. One may come from the dual-solution characteristics of the shock–combustion interaction in test A1 with $\Delta\Phi_h = 0.07$. And the other may come from the historical effect of reverse flow with oscillation in test A2 with $\Delta\Phi_h = 0.16$. Compared to the shock–combustion interaction type in test A1, the reverse flow type in test A2 requires greater downstream heat release and generates a larger hysteresis loop. In other words, the unstart degree will alter the inlet restart characteristics in the scramjet due to the combustion effect.

In addition, the change characteristics of the thrust increment in tests A1 and A2 are different. The thrust increment in test A1 exhibits a nearly linear change as ER varies, but the change characteristics of the thrust increment in test A2 are more complicated. Corresponding to the formation of the reverse flow, an abrupt increase in the pressure brings an abrupt drop and large oscillation to the energy thrust. And then, the thrust increment starts to increase due to the shrinking amplitude and range of the high-pressure zone in the inlet and reaches the maximum value at the critical moment when the reverse flow disappears. Therefore, once the unstart/restart hysteresis phenomenon accompanied by the reverse flow occurs in actual flight, the thrust variation coupling with the flight speed, height, and attitude of the vehicle, will make the engine more difficult to restart.

Consequently, the coupling effect between the upstream aerodynamic flow and the downstream combustion weakens the inlet restart capability in the scramjet. The specific mechanism of the coupling effect will vary with the flow structure and combustion intensity. Therefore, more work is needed to decouple the two factors scientifically.

ACKNOWLEDGMENTS

AUTHOR DECLARATIONS
Conflict of Interest

The authors have no conflicts to disclose.

Author Contributions

Qifan Zhang: Formal analysis (lead); Writing – original draft (lead). **Hao Chen:** Funding acquisition (lead); Writing – review and editing (lead). **Zhenjie Wu:** Investigation (supporting); Writing – original draft (supporting). **Zhanbiao Gao:** Software (lead). **Weihang Luo:** Visualization (lead). **Hongbin Gu:** Software (supporting). **Lianjie Yue:** Conceptualization (lead); Funding acquisition (supporting).

DATA AVAILABILITY

The data that support the findings of this study are available from the corresponding authors upon reasonable request.

REFERENCES

[1]D. Van Wie, "Scramjet inlets," in *Scramjet Propulsion*, edited by E. T. Curran and S. N. B. Murthy (AIAA, Reston, 2000), pp. 447–504.

[2]T. A. Emami, H. Auslender, and P. Weidner, "Experimental investigation of inlet-combustor isolators for a dual-mode scramjet at a Mach number of 4," Report No. NASA TP-3502 (NASA, Washington, D.C., 1995).

[3]A. K. Flock and A. Gülhan, "Experimental investigation of the starting behavior of a three-dimensional scramjet intake," AIAA J. **53**(9), 2686–2693 (2015).

[4]K. L. Liu and K. Y. Zhang, "Unsteady start/unstart characteristics of 2-D hypersonic inlet caused by oscillating angle of attack," J. Propuls. Technol. **31**(6), 676–680 (2010) (in Chinese).

[5]M. Bolender, H. Wilkin, L. Jacobsen, T. Drayna, and A. Dwenger, "Flight dynamics of a hypersonic vehicle during inlet un-start," AIAA Paper No. 2009-7292, 2009.

[6]R. Voland, A. Auslender, M. Smart, A. Roudakov, V. Semenov, and V. Kopchenov, "CIAM/NASA Mach 6.5 scramjet flight and ground test," AIAA Paper No. 1999-4848, 1999.

[7]G. Norris, "X-51A scramjet fails on second attempt," Aerospace Daily and Defense Report, **238**(55), (2011); available at https://aviationweek.com/x-51a-scramjet-fails-second-attempt.

[8]K. Oswatitsch, "Pressure recovery for missiles with reaction propulsion at high supersonic speeds (the efficiency of shock diffusers)," Report No. NACA-TM-1140 (NASA, Washington, D.C., 1944).

[9]H. J. Tan, S. Sun, and Z. L. Yin, "Oscillatory flows of rectangular hypersonic inlet unstart caused by downstream mass-flow choking," J. Propuls. Power **25**(1), 138–147 (2009).

[10]H. J. Tan, L. G. Li, Y. F. Wen, and Q. F. Zhang, "Experimental investigation of the unstart process of a generic hypersonic inlet," AIAA J. **49**(2), 279–288 (2011).

[11]J. L. Wagner, K. B. Yuceil, A. Valdivia, N. T. Clemens, and D. S. Dolling, "Experimental investigation of unstart in an inlet/isolator model in Mach 5 flow," AIAA J. **47**(6), 1528–1542 (2009).

[12]J. L. Wagner, K. B. Yuceil, and N. T. Clemens, "Velocimetry measurements of unstart of an inlet-isolator model in Mach 5 flow," AIAA J. **48**(9), 1875–1888 (2010).

[13]Z. F. Li, W. Z. Gao, H. L. Jiang, and J. M. Yang, "Unsteady behaviors of a hypersonic inlet caused by throttling in shock tunnel," AIAA J. **51**(10), 2485–2492 (2013).

[14]J. T. Chang, L. Wang, W. Bao, J. Qin, J. Niu, and W. Xue, "Novel oscillatory patterns of hypersonic inlet buzz," J. Propuls. Power **28**(6), 1214–1221 (2012).

[15]H. J. Tan and R. W. Guo, "Experimental study of the unstable-unstarted condition of a hypersonic inlet at Mach 6," J. Propuls. Power **23**(4), 783–788 (2007).

[16]C. P. Wang, L. S. Xue, and K. M. Cheng, "Novel inducement to unstart of a parallel modular hypersonic inlet," AIAA J. **57**(2), 760–771 (2019).

[17]Q. F. Zhang, H. J. Tan, S. Sun, H. X. Bu, and C. Y. Rao, "Unstart of a hypersonic inlet with side compression caused by downstream choking," AIAA J. **54**(1), 28–38 (2016).

[18]Y. Tao, W. D. Liu, X. Q. Fan, and Y. L. Zhao, "Structural characteristics of the shock-induced boundary layer separation extended to the leading edge," Phys. Fluids **29**, 071701 (2017).

[19]M. K. K. Devaraj, P. Jutur, S. M. V. Rao, G. Jagadeesh, and G. T. K. Anavardham, "Experimental investigation of unstart dynamics driven by subsonic spillage in a hypersonic scramjet intake at Mach 6," Phys. Fluids **32**, 026103 (2020).

[20]K. R. Sekar, S. K. Karthick, S. Jegadheeswaran, and R. Kannan, "On the unsteady throttling dynamics and scaling analysis in a typical hypersonic inlet-isolator flow," Phys. Fluids **32**, 126104 (2020).

[21]J. T. Chang, N. Li, K. J. Xu, W. Bao, and D. R. Yu, "Recent research progress on unstart mechanism, detection and control of hypersonic inlet," Prog. Aerosp. Sci. **89**, 1–22 (2017).

[22]S. O'Byrne, M. Doolan, S. R. Olsen, and A. F. P. Houwing, "Analysis of transient thermal choking processes in a model scramjet engine," J. Propuls. Power **16**(5), 808–814 (2000).

[23]S. J. Laurence, S. Karl, J. Martinez Schramm, and K. Hannemann, "Transient fluid-combustion phenomena in a model scramjet," J. Fluid Mech. **722**, 85–120 (2013).

[24]S. J. Laurence, D. Lieber, J. M. Schramm, K. Hannemann, and J. Larsson, "Incipient thermal choking and stable shock-train formation in the heat-release region of a scramjet combustor. Part I: Shock-tunnel experiments," Combust. Flame **162**(4), 921–931 (2015).

[25]Q. L. Liu, A. Passaro, D. Baccarella, and H. Do, "Ethylene flame dynamics and inlet unstart in a model scramjet," J. Propuls. Power **30**(6), 1577–1585 (2014).

[26]D. Baccarella, Q. Liu, B. McGann, G. Lee, and T. Lee, "Isolator-combustor interactions in a circular model scramjet with thermal and non-thermal choking-induced unstart," J. Fluid Mech. **917**, A38 (2021).

[27]S. Im, D. Baccarella, B. McGann, Q. Liu, L. Wermer, and H. Do, "Unstart phenomena induced by mass addition and heat release in a model scramjet," J. Fluid Mech. **797**, 604–629 (2016).

[28]L. J. Yue, Y. N. Jia, X. Xu, X. Y. Zhang, and P. Zhang, "Effect of cowl shock on restart characteristics of simple ramp type hypersonic inlets with thin boundary layers," Aerosp. Sci. Technol. **74**, 72–80 (2018).

[29]R. W. Cubbison and G. Mitchell, "An experimental investigation of the restart area ratio of a Mach 3.0 axisymmetric mixed compression inlet," Report No. NASA TM-X-1547 (NASA, Washington, D.C., 1968).

[30]J. You, A. Y. Yu, J. L. Le, S. H. Yang, X. S. Rong, and F. J. Li, "Experimental research on restarting characteristics of supersonic inlet based of injection regulation," AIAA Paper No. 2017-2387, 2017.

[31]H. X. Huang, H. J. Tan, J. Cai, and S. Sun, "Restart processes of rectangular hypersonic inlets with different internal contraction ratios," AIAA J. **59**(7), 2427–2439 (2021).

[32]J. T. Chang, L. Wang, W. Bao, Q. C. Yang, and J. Qin, "Experimental investigation of hysteresis phenomenon for scramjet engine," AIAA J. **52**(2), 447–451 (2014).

[33]B. Qin, J. T. Chang, X. L. Jiao, and W. Bao, "Unstart margin characterization method of scramjet considering isolator-combustor interactions," AIAA J. **53**(2), 493–500 (2015).

[34]Z. J. Wu, Q. F. Zhang, X. Zhang, W. H. Luo, Z. B. Gao, and L. J. Yue, "Experimental investigation of abrupt change in a scramjet with variable Mach-number flow," AIAA J. **60**(7), 4006–4014 (2022).

[35]X. Zhang, L. J. Yue, T. L. Huang, Q. F. Zhang, and X. Y. Zhang, "Numerical investigation of mode transition and hysteresis in a cavity-based dual-mode scramjet combustor," Aerosp. Sci. Technol. **94**, 105420 (2019).

[36]X. Zhang, Q. F. Zhang, Z. J. Wu, L. J. Yue, Z. B. Gao, W. H. Luo, and H. Chen, "Experimental study of hysteresis and catastrophe in a cavity-based scramjet combustor," Chin. J. Aeronaut. (published online, 2022).

[37]Q. F. Zhang, H. J. Tan, H. Chen, Y. Q. Yuan, and Y. C. Zhang, "Unstart process of a rectangular hypersonic inlet at different Mach numbers," AIAA J. **54**(12), 3681–3691 (2016).